Bayesian generalized linear AVA inversion for VTI media

Xin Fu, Kris Innanen

ABSTRACT

The research in this paper is to realize the simultaneous AVA (amplitude variation with angle) inversion of anisotropic parameters for the transversely isotropic media with vertical axis of symmetry (VTI media). First, we introduce a nonlinear PP-wave reflection coefficient approximation equation called ASI equation for isotropic elastic media. Then by replacing the isotropic part of Rüger equation with this equation, we obtain a new PP-wave reflection coefficient approximation equation called ASI Rüger equation for VTI media. In order to invert the VTI parameters based on ASI Rüger equation, we develop the Bayesian generalized linear inversion (BGLI), in which the noise and model perturbation are assumed to conform to the zero mean Gaussian distribution. ASI Rüger equation can express the PP-wave reflection coefficient in VTI media well. Compared with Rüger equation, ASI Rüger equation demonstrates less sensitivity to the bias in the intrinsic constant, lowers the relevance between the parameters, and reduces the ill-posedness of inversion problem. The synthetic data test shows that the proposed method can stably and reliably invert VTI parameters (the vertical P-wave impedance, the vertical S-wave impedance, Thomsen's parameters δ and ϵ) , and the inverted results are almost unaffected by the errors in the intrinsic constant.

INTRODUCTION

Amplitude versus angle (AVA) or amplitude versus offset (AVO) prestack seismic inversion, a widely used technology in the oil and gas industry (Castagna and Backus, 1993), is playing an important role and has been applied successfully. The fundamental basis for this approach is Zoeppritz equation (Zoeppritz, 1919) which provides the exact epression of reflection coefficients for elastic isotropic media. However, the high computation cost and the strong nonlinearity of Zoeppritz equation hampered its use in the AVO/AVA prestack inversion in the past. In orther to ralize AVO/AVA inversion, many simplified approximation equations to Zoeppritz equation have derived (Bortfeld, 1961; Richards and Frasier, 1976; Aki and Richards, 2002; Wiggins et al., 1983; Shuey, 1985; Smith and Gidlow, 1987; Gidlow et al., 1992; Mallick, 1993; Fatti et al., 1994; Goodway et al., 1997; Gray et al., 1999; Wang, 1999; Russell et al., 2011; Zong et al., 2013; Fu et al., 2018). With the increasing requirements of seismic exploration, more-accurate approximations of reflection coefficients are proposed (Wang, 1999; Stovas and Ursin, 2001; Ursenbach, 2002; Innanen, 2011, 2013; Innanen and Mahmoudian, 2015). Even, some researchers directly employ the exact Zoeppritz equations to perform the prestack inversion (Liu et al., 2011; Wei and Chen, 2011; Zhu and McMechan, 2012; Ma et al., 2013; Zhi et al., 2016; Zhou et al., 2017; Pan et al., 2017; Gholami et al., 2018), which benefits from the development of computer power.

Although the exact reflection coefficient equation for isotropic media can be employed, the anisotropic property of subsurface rocks sometimes cannot be ignored. Thomsen (1986) shows that most subsurface rocks are weakly anisotropic and proposes three parameters (Thomsen's parameters: δ, ϵ, and γ) to describe the anisotropic property of transversely

isotropic media. Wright (1987) reports that the vertical and horizontal P-wave velocities of the deltaic sand-shale sequences can vary by up to 20 percent due to the anisotropy. And the effects of transverse isotropy can lead to obvious changes to the reflection coefficients (Kim et al., 1993) even the reversal of the reflection trend (Carcione et al., 1998). For the importance of the anisotropy, many formulas to depict the reflection coefficients in isotropic media have been derived (Keith and Crampin, 1977; Fryer and Frazer, 1984; Vavrycuk and Psencik, 1998; Zillmer et al., 1998; Zhang and Li, 2013). The version of Zoeppritz equation for the transversely isotropic media are given by , Daley and Hron (1977), Graebner (1992), and Schoenberg and Protazio (1992). And its approximations are derived as well (Banik, 1987; Rüger, 1997, 1998; Stovas and Ursin, 2003; Jin and Stovas, 2019), which enable to directly understand the anisotropy behavior and more easily inverse the parameters about anisotropic properties.

As a tipical anistropical type, the transversely isotropic media with vertical axis of symmetry (VTI media) is significant to hydrocarbon industries, since it involves horizontal thin interbed reservoir and horizontal cracks, etc. A famous reflection coefficient approximation for VTI media is Rüger equation (Rüger, 1997), which is expressed by Thomsen's anisotropy parameters (Thomsen, 1986). However, the AVA inversion of using straightly Rüger equation has not been realized because of the strong ill-posedness and the coupling between parameters (Plessix and Bork, 2000). Several researchers presents the indirect methods to invert anisotropic parameters. (Stovas et al., 2006) estimate net-to-gross (N/G) and oil saturation using AVO attributes (intercept and gradient) based on the thin-layer reflectivity modeling. Lin and Thomsen (2013) estimate δ from the difference between measured seismic data and synthetic data calculated by well logs. Based on a modified Rüger equation, Zhang et al. (2019) present a rock-physics-based method and a stepwise-inversion-based method, which inverse the Thomsen's parameter ϵ.

To realize the simultaneous AVA inversion of anisotropic parameters (δ, ϵ) for VTI media, we present a new method based upon a new PP-wave reflection coefficient approximation equation for VTI media which is a combination of two equations, one is a nonlinear PP-wave reflection coefficient approximation equation for isotropic elastic media, the other one is Rüger equation. In this paper, first, we instroduce the nonlinear approximation equation for isotropic elastic media. Next it is used to replace the isotropic part of Rüger equation, which generates the new PP-wave reflection coefficient approximation equation for VTI media. After that we introduce Bayesian generalized linear inversion algorithm. Furthermore, we systematically analysis the new equation and compare it with Rüger equation. Finally, we use synthetic data with different noise levels to test the proposed method.

FORWARD MODELING THEORY

Reflection coefficients in isotropic media

Exact reflection coefficients for isotropic elastic media are given by Zoeppritz equation (Zoeppritz, 1919). Following it, many approximation equations have been derived. These have the purposes of inversing different parameters, steadying inversion algorithms, and enhancing the accuracy of inverted results. In this section, we derive a new PP-wave reflectivity approximation equation in isotropic AVO inversion. We start from a two-term

approximation equation expressed as a function of ray parameter p (Mallick, 1993; Wang, 1999):

$$R(p) = R_f(p) + R_g(p), \tag{1}$$

where

$$\begin{aligned} R_f(p(\theta)) &= \frac{\rho_2\alpha_2/\cos\theta_t - \rho_1\alpha_1/\cos\theta}{\rho_2\alpha_2/\cos\theta_t + \rho_1\alpha_1/\cos\theta}\ (fluid - fluid\ term) \\ R_g(p(\overline{\varphi})) &= -2\frac{\Delta\mu}{\overline{\rho}} \approx -2(\frac{\Delta\rho}{\overline{\rho}} + 2\frac{\Delta\beta}{\overline{\beta}})\tan^2\overline{\varphi}\cos^2\overline{\varphi}\ (rigidity\ term) \end{aligned} \tag{2}$$

where $p = sin\theta/\alpha_1 = sin\varphi/\beta_1$ represents ray parameter; $R_f(p(\theta))$ represents the reflection coefficients associated with pore fluid at the reflection interface, which is called as fluid-fluid term, where θ and θ_t represent incident angle and transmission angle of PP wave, respectively, and α_1, β_1, ρ_1, α_2, β_2, ρ_2 are P-wave velocity, S-wave velocity and density of upper and lower media of the interface, respectively; $R_g(p)$ is called as rigidity term (Hilterman, 2001), where $\Delta\mu = \overline{\beta}^2\Delta\rho + 2\overline{\rho}\overline{\beta}\Delta\beta$ is the difference between the shear modulus of the upper and lower media of the interface, $\overline{\beta} = (\beta_2 + \beta_1)/2$, $\overline{\rho} = (\rho_2 + \rho_1)/2$, $\Delta\beta = \beta_2 - \beta_1$, $\Delta\rho = \rho_2 - \rho_1$, and $\overline{\varphi} = (\varphi_t + \varphi)/2$ is the average of P-SV wave reflection angle φ and transmission angle φ_t.

According to Potter and Stewart (1998), the ratio of density reflectivity to S-wave reflectivity can be expressed as a constant of $r = (\Delta\rho/\overline{\rho})/(\Delta\beta/\overline{\beta})$. Putting this formula and the approximate formula of $\Delta\varphi = \varphi_t - \varphi \approx \frac{\Delta\beta}{\overline{\beta}}\tan\overline{\varphi}$ (Aki and Richards, 2002) into the rigidity term, we have the flowing:

$$R_g(p(\varphi)) \approx -2(2+r)\cos^2\overline{\varphi}\tan^2\overline{\varphi}\frac{\Delta\beta}{\overline{\beta}} \approx -2(2+r)\cos^2\overline{\varphi}\tan^2\overline{\varphi}\Delta\varphi, \tag{3}$$

where $\tan\overline{\varphi}\Delta\varphi$ is approximated by Wang (2003) and Ma (2003) as flows:

$$\tan\overline{\varphi}\Delta\varphi = \frac{\sin\overline{\varphi}}{\cos\overline{\varphi}}\Delta\varphi \approx -\frac{\Delta\cos\varphi}{\overline{\cos\varphi}} \approx -\ln\frac{\cos\varphi_t}{\cos\varphi}, \tag{4}$$

where $\Delta\cos\varphi = \cos\varphi_t - \cos\varphi$, $\overline{\cos\varphi} = (\cos\varphi_t + \cos\varphi)/2$.

By inserting equation 4 into equation 3 , we can obtain the rigidity term as a logarithmic form:

$$R_g(p(\varphi)) \approx 2(r+2)\cos^2\overline{\varphi}\ln\frac{\cos\varphi_t}{\cos\varphi} = (r+2)\ln\frac{\cos^{2\cos^2\overline{\varphi}}\varphi_t}{\cos^{2\cos^2\overline{\varphi}}\varphi}. \tag{5}$$

To further simplify this equation and lessen the number of parameters, the $\cos\overline{\varphi}$ in the numerator of the logrithmic term is approximated as $\cos\varphi_t$, the $\cos\overline{\varphi}$ in the denominater of the logrithmic term is approximated as $\cos\varphi$, then

$$R_g(p(\varphi)) \approx (r+2)\ln\frac{\cos^{2\cos^2\varphi_t}\varphi_t}{\cos^{2\cos^2\varphi}\varphi} \approx 2(r+2)\frac{\cos^{2\cos^2\varphi_t}\varphi_t - \cos^{2\cos^2\varphi}\varphi}{\cos^{2\cos^2\varphi_t}\varphi_t + \cos^{2\cos^2\varphi}\varphi}. \tag{6}$$

According to Snell's law:

$$\begin{aligned}\cos^2\varphi_t &= 1-\sin^2\varphi_t = 1-\frac{\beta_2^2}{\alpha_2^2}\sin^2\theta_t,\\ \cos^2\varphi &= 1-\sin^2\varphi = 1-\frac{\beta_1^2}{\alpha_1^2}\sin^2\theta.\end{aligned} \tag{7}$$

after putting equation 7 into equation 6, we obtain:

$$R_g(p(\theta)) \approx 2(r+2)\frac{(1-\frac{\beta_2^2}{\alpha_2^2}\sin^2\theta_t)^{1-\frac{\beta_2^2}{\alpha_2^2}\sin^2\theta_t} - (1-\frac{\beta_1^2}{\alpha_1^2}\sin^2\theta)^{1-\frac{\beta_1^2}{\alpha_1^2}\sin^2\theta}}{(1-\frac{\beta_2^2}{\alpha_2^2}\sin^2\theta_t)^{1-\frac{\beta_2^2}{\alpha_2^2}\sin^2\theta_t} + (1-\frac{\beta_1^2}{\alpha_1^2}\sin^2\theta)^{1-\frac{\beta_1^2}{\alpha_1^2}\sin^2\theta}}. \tag{8}$$

Finally, in equation 8, the ratios of S- to P-wave velocity, β_1/α_1 and β_2/α_2, are respectively written as the ratios of S- to P-wave impedance, SI_1/AI_1 and SI_2/AI_2 ($SI_1=\beta_1\rho_1$, $SI_2=\beta_2\rho_2$, $AI_1=\alpha_1\rho_1$, $AI_2=\alpha_2\rho_2$), then the reflection coefficient of the reflection interface (equation 1) can be expressed as a function of P-wave impedance (or acoustic impedance) and S-wave impedance:

$$\begin{aligned}R_{ASI}(p(\theta)) = R_f(p(\theta)) + R_g(p(\theta)) &\approx \frac{AI_2/\cos\theta_t - AI_1/\cos\theta}{AI_2/\cos\theta_t + AI_1/\cos\theta}\\ &+ 2(r+2)\frac{(1-\frac{SI_2^2}{AI_2^2}\sin^2\theta_t)^{1-\frac{SI_2^2}{AI_2^2}\sin^2\theta_t} - (1-\frac{SI_1^2}{AI_1^2}\sin^2\theta)^{1-\frac{SI_1^2}{AI_1^2}\sin^2\theta}}{(1-\frac{SI_2^2}{AI_2^2}\sin^2\theta_t)^{1-\frac{SI_2^2}{AI_2^2}\sin^2\theta_t} + (1-\frac{SI_1^2}{AI_1^2}\sin^2\theta)^{1-\frac{SI_1^2}{AI_1^2}\sin^2\theta}}.\end{aligned} \tag{9}$$

Since formula 9 establishes the relationship between PP-wave reflection coefficient and P-wave impedance (or acoustic impedance) and S-wave impedance, we call it as ASI equation, and the reflection coefficient is noted as R_{ASI}.

As a nonlinear equation employed to inverse P- and S-wave impedances simultaneously (Fu et al., 2017, 2019), ASI equation (equation 9) only contains P-wave and S-wave impedances, which reduces the number of parameters and helps to stabilize the inversion algorithm by reducing the ill-posedness of the inverse problem, but does not lower the expression accuracy of PP wave reflectivity. And the impact to inverted results caused by error of the intrinsic constant in ASI equation is much smaller than that in the other approximate equations in which the S- to P-wave velocity ratio is assumed as a constant. For more analysis and applications about ASI equation, readers can refer to Fu et al. (2017, 2019). Furthermore, this equation can also be utilized to simultaneously estimate other parameters which can be expressed by P- and/or S-wave impedances, e.g. P-wave impedance and the ratio of S- to P-wave velocity (Fu et al., 2018).

Reflection coefficients in the transversely isotropic media with vertical axis of symmetry

Anisotropy is a common property in underground rocks and one reasons that affects the reflection coefficient of seismic waves. And the influence of anisotropy on seismic data sometimes cannot be ignored. The transversely isotropic media with vertical axis of symmetry (VTI media) is one of the most typical anisotropic media. Based on the assumption that the anisotropy is weak, a linear approximation formula for PP-wave reflection coefficient in VTI media, which is expressed by Thomsen's anisotropy parameters (Thomsen, 1986), is given by Rüger (1997):

$$R_p^{VTI}(\theta) = \frac{1}{2}\frac{\Delta AI}{\overline{AI}} - 2k^2 \sin^2\theta \frac{\Delta\mu}{\overline{\mu}} + \frac{1}{2}\tan^2\theta\frac{\Delta\alpha}{\overline{\alpha}} + \frac{1}{2}\sin^2\theta\Delta\delta + \frac{1}{2}\sin^2\theta\tan^2\theta\Delta\epsilon, \tag{10}$$

$$\begin{aligned}
&\Delta AI = \alpha_2\rho_2 - \alpha_1\rho_1,\ \Delta AI = \alpha_2\rho_2 - \alpha_1\rho_1,\\
&\Delta\mu = \rho_2\beta_2^2 - \rho_1\beta_1^2,\ \overline{\mu} = (\rho_2\beta_2^2 + \rho_1\beta_1^2)/2,\\
&\Delta\alpha = \alpha_2 - \alpha_1,\ \overline{\alpha} = (\alpha_2 + \alpha_1)/2,\\
&\Delta\delta = \delta_2 - \delta_1,\ \Delta\epsilon = \epsilon_2 - \epsilon_1,\\
&k = \frac{\overline{\beta}}{\overline{\alpha}},\ \overline{\beta} = (\beta_2 + \beta_1)/2,
\end{aligned}$$

where θ represents the incidence phase angle of the reflection interface, AI represents the vertical P-wave impedance, μ represents the vertical shear modulus, and α_1, β_1, ρ_1, α_2, β_2, ρ_2 are the vertical P-wave velocity, the vertical S-wave velocity and the bulk density of the upper and lower media of the reflection interface, respectively. In formular 10, k is the velocity ratio usually assumed as a constant during the prestack inversion. δ and ϵ are two of Thomsen's three anisotropic parameters, δ_1, ϵ_1, ,δ_2, ϵ_2 are the two anisotropic parameters of the upper and lower media of the reflection interface.

Since equation 10 contains too many parameters , the ill-posedness of the inverse problem of using it is too strong, it means the anisotropic parameters cannot be inverted simultaneously. Because equation 9 had the advantages of reducing the number in parameters and the ill-posedness of the inverse problem, we can utilize this equation to estimate the anisotropic parameters. For the reason that both of equation 9 and the isotropic part (the first three terms) in equation 10 are the approximations of Zoeppritz equation for isotropic elastic media, it is reasonable to replace the isotropic part of equation 10 with equation 9. After the replacement, we have a new PP-wave reflection coefficient approximation in VTI

media:

$$R_{ASI}^{VTI}(\theta) = \frac{AI_2/\cos\theta_t - AI_1/\cos\theta}{AI_2/\cos\theta_t + AI_1/\cos\theta} + 2(r+2)\frac{(1-\frac{SI_2^2}{AI_2^2}\sin^2\theta_t)^{1-\frac{SI_2^2}{AI_2^2}\sin^2\theta_t} - (1-\frac{SI_1^2}{AI_1^2}\sin^2\theta)^{1-\frac{SI_1^2}{AI_1^2}\sin^2\theta}}{(1-\frac{SI_2^2}{AI_2^2}\sin^2\theta_t)^{1-\frac{SI_2^2}{AI_2^2}\sin^2\theta_t} + (1-\frac{SI_1^2}{AI_1^2}\sin^2\theta)^{1-\frac{SI_1^2}{AI_1^2}\sin^2\theta}} + \frac{1}{2}\sin^2\theta\Delta\delta + \frac{1}{2}\sin^2\theta\tan^2\theta\Delta\epsilon. \tag{11}$$

It should be noted that since the equation is applicable to weakly anisotropic VTI media, the parameters in the isotropic part are the ones at zero incident phase angle, the vertical parameters. In particular, when θ is the incidence phase angle, θ_t is not the true transmission phase angle in VTI media, but the transmission angle in isotropic background media, they are applicable to the relationship of $\frac{\sin\theta_t}{\sin\theta} = \frac{\alpha_2}{\alpha_1}$, the Snell's law for isotropic media. Later, we will analyze this equation systematically. Cause equation 11 is a combination of ASI equation (equation 9) and Rüger equation (equation 10), we call it ASI Rüger equation, noted as R_{ASI}^{VTI}.

BAYESIAN GENERALIZED LINEAR INVERSION

In this section we introduce Bayesian generalized linear inversion (BGLI) algorithm which is a conbination of generalized linear inversion (GLI) and Bayesian linear inversion (BLI). In this algorithm, the GlI theory is employed to transform the nonlinear problem into a linear problem, and then the BLI theory is employed to minimize the objective function and maximize the likelihood function.

ASI Rüger equation is a nonlinear equation, to avoid the high-cost nonlinear inversion algorithms, we adopt the generalized linear inversion method (GLI) introduced by Cooke and Schneider (1983). The GLI method considers data $\mathbf{d}$ as a nonlinear function of true model $\mathbf{m}$, after expending this function in a Taylor series about an initial model $\mathbf{m}_0$ and keeping the linear part only, we have:

$$\mathbf{d}(\mathbf{m}) = \mathbf{d}(\mathbf{m}_0) + \frac{\partial\mathbf{d}(\mathbf{m}_0)}{\partial\mathbf{m}_0}(\mathbf{m}-\mathbf{m}_0) + \mathbf{n}. \tag{12}$$

where, for our problem, $\mathbf{d}(\mathbf{m})$ is prestack angle gather dataset, $\mathbf{d}(\mathbf{m}_0)$ is the synthetic data calculated, based on the convolution model, by using the initial model $\mathbf{m}_0$, wavelets, and ASI Rüger equation, and $\frac{\partial\mathbf{d}(\mathbf{m}_0)}{\partial\mathbf{m}_0}$ is the partial derivative matrix or Jacobian matrix of $\mathbf{d}(\mathbf{m}_0)$ with respect to $\mathbf{m}$ at $\mathbf{m} = \mathbf{m}_0$, and $\mathbf{n}$ is the noise in $\mathbf{d}(\mathbf{m})$. For the specific expressions of these symbols, please refer to Appendix A.

Let $\Delta\mathbf{d} = \mathbf{d}(\mathbf{m}) - \mathbf{d}(\mathbf{m})_0$, $\Delta\mathbf{m} = \mathbf{m} - \mathbf{m}_0$, and $\mathbf{G} = \frac{\partial\mathbf{d}(\mathbf{m}_0)}{\partial\mathbf{m}_0}$, equation 12 is rewritten

as:

$$\Delta\mathbf{d} = \mathbf{G}\Delta\mathbf{m} + \mathbf{n}. \tag{13}$$

Bayes formula can be expressed as:

$$P(\mathbf{x}|\mathbf{d}^{'}) = \frac{P(\mathbf{d}^{'}|\mathbf{x})P(\mathbf{x})}{P(\mathbf{d}^{'})} \propto P(\mathbf{d}^{'}|\mathbf{x})P(\mathbf{x}), \tag{14}$$

where $d^{'}$ is the known dataset, $\mathbf{x}$ is the model to be solved, $P(\mathbf{d}^{'})$ is a constant, $P(\mathbf{x}|\mathbf{d}^{'})$ is posterior probability distribution function, $P(\mathbf{d}^{'}|\mathbf{x})$ is likelihood function that represents the conditional probability distribution of the known dataset when the model is determined, $P(\mathbf{x})$ is a prior probability distribution. For equation 13, $d^{'}$ represents $\Delta\mathbf{d}$, $\mathbf{x}$ represents $\Delta\mathbf{m}$. Assuming that the noise $\mathbf{n} = \Delta\mathbf{d} - \mathbf{G}\Delta\mathbf{m}$ in equation 13 conforms to the zero mean Gaussian distribution, and the model perturbation $\Delta\mathbf{m}$ also conforms to the zero mean Gaussian distribution, then the posterior probability distribution $P(\Delta\mathbf{m}|\Delta\mathbf{d})$ can be expressed as:

$$\begin{aligned} P(\Delta\mathbf{m}|\Delta\mathbf{d}) &\propto P(\Delta\mathbf{d}|\Delta\mathbf{m})P(\Delta\mathbf{m}) \\ &\propto \frac{1}{\sigma_n\sqrt{2\pi}}\exp[-\frac{(\Delta\mathbf{d}-\mathbf{G}\Delta\mathbf{m})^T(\Delta\mathbf{d}-\mathbf{G}\Delta\mathbf{m})}{2\sigma_n^2}] \\ &\times \frac{1}{(\sqrt{2\pi})^m\sqrt{|\mathbf{C}_{\Delta m}|}}\exp(-\frac{\Delta\mathbf{m}^T\mathbf{C}_{\Delta m}^{-1}\Delta\mathbf{m}}{2}) \\ &\propto exp[-\frac{(\Delta\mathbf{d}-\mathbf{G}\Delta\mathbf{m})^T(\Delta\mathbf{d}-\mathbf{G}\Delta\mathbf{m})}{2\sigma_n^2} - \frac{\Delta\mathbf{m}^T\mathbf{C}_{\Delta m}^{-1}\Delta\mathbf{m}}{2}], \end{aligned} \tag{15}$$

where σ_n is the standard deviation of error term $\mathbf{n}$, m is the dimension number of the model, and $\mathbf{C}_{\Delta m}$ is the covariance matrix of Δm represented as:

$$\mathbf{C}_{\Delta m} = Kron(Cov\{\Delta\mathbf{AI}, \Delta\mathbf{SI}, \Delta\boldsymbol{\delta}, \Delta\boldsymbol{\epsilon}\}, \mathbf{I}), \tag{16}$$

where $Kron(\cdot)$ is the Kronecker product, $Cov(\cdot)$ is the covariance matrix, and $\mathbf{I}$ is the identity matrix of $(l+1)\times(l+1)$, when $(l+1)$ is the length of the parameter perturbations, $\Delta\mathbf{AI}$, $\Delta\mathbf{SI}$, $\Delta\boldsymbol{\delta}$, or $\Delta\boldsymbol{\epsilon}$ (See Appendix A). From the initial model $\mathbf{m}_0$ and real log data, $\mathbf{C}_{\Delta m}$ can be obtained at the well location, which needs to be calculated in each inversion iteration.

In order to maximize the posterior probability, objective function is obtained by taking logarithm on both sides of formula 15, and then let the derivative of the objective function with respect to model perturbation be zero to minimize the the objective function, so the model perturbation in each iteration can expressed as:

$$\Delta\mathbf{m} = (\mathbf{G}^T\mathbf{G} + \lambda\mathbf{C}_{\Delta m}^{-1})^{-1}\mathbf{G}^T\Delta\mathbf{d}, \tag{17}$$

where σ_n is absorbed into the trade-off parameter λ which controls the relative importance of data and prior information. Finally, the inverted model can be obtained by the following formula:

$$\mathbf{m} = \mathbf{m}_0 + \Delta\mathbf{m}. \tag{18}$$

Because ASI Rüger equation includes both the incident angle θ_i, and the transmission angle θ_{i+1} in isotropic background media, whereas the data we are using is angle gather, which means that only the incident angle information is available. So before inversing, we use Snell's law to obtain the transmission angle in the istropic background media, as follow:

$$\theta_t = \sin^{-1}(\frac{\alpha_2}{\alpha_1}\sin\theta), \tag{19}$$

where if α_1 is the vertical P-wave velocity of i^{th} layer, α_2 is the vertical P-wave velocity of $i+1^{th}$ layer, both of them come from the initial vertical P-wave velocity model.

THE ANALYSIS OF REFLECTION COEFFICIENT EQUATIONS

The ASI Rüger equation is analyzed systematically from the following four aspects: (1) expression accuracy analysis; (2) the influence of intrinsic constant on reflection coefficients; (3) the contribution of parameters to reflection coefficients; (4) sensitivity matrix analysis.

To analyse the accuracy of ASI Rüger equation, we use four single-interface AVO models in Table 1 and have comparisons with the eaxct reflectivity equation and Rüger equation. In Table 1, the AVO model 1, 2, and 3 is class I, class II, and class III (Rutherford and Williams, 1989), respectively, used by Zhang et al. (2019), and the model 4 is used by Rüger (1997). Figure 1 shows the reflection coefficients of these models, the reflection coefficients for each model are computed by the exact reflection coefficient equation for VTI media (Schoenberg and Protazio, 1992), Rüger equation, ASI Rüger equation and the isotropic parts of them. The isotropic part of ASI Rüger equation is equation 9. From the accuracy comparisons of Figure 1, it can be seen that both of Rüger equation and ASI Rüger equation have good reflection coefficient expression accuracy in VTI media.

The intrinsic constant in reflection coefficient equations is a crucial factor that affects the accuracy of inversion results. Usually, the vertical S- to P-wave velocity ratio (k) in a linear reflection coefficient approximation, such as equation 10, is set as a constant during the inversion. Similarly, during the inversion, the ratio of density reflectivity to S-wave reflectivity (r) in ASI Rüger equation is also set as a constant. In order to investigate how the constant impacts the expression accuracy of ASI Rüger equation, we use ASI Rüger equation and different r values to obtain reflection coefficients , and compared them with that by using Rüger equation and different k values. The parameters used are from model 2 in Table 1. The curves are shown in Figure 2. The comparison shows that ASI Rüger equation is much less sensitive to the intrinsic constant than Rüger equation. It also indirectly indicates that the inversion results are less affected by the constant assumption.

The contribution of each parameter to the reflection coefficient is another important index to appraise the inversion capability of the reflection coefficient equation. The more relevant the parameters are, the more difficult it is to separate in the inverted results (Plessix and Bork, 2000; Zong et al., 2015). In Figure 3, we show the PP-wave reflection coefficients for a single interface of model 2 in Table 1 using Rüger equation, in each subgraph of Figure 3, only one parameter is varied when the other nine are fixed. Similarly, in Figure 4, we show the PP-wave reflection coefficients for model 2 using ASI Rüger equation, in

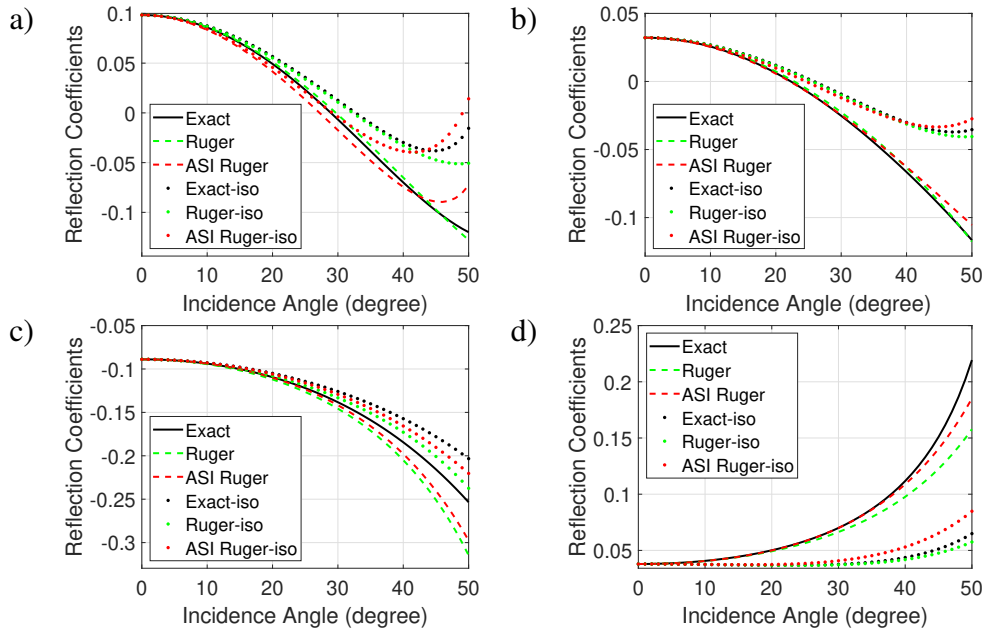

FIG. 1. The PP-wave reflection coefficients of four single-interface models in Table 1: (a) model 1, (b) model 2, (c) model 3, (d) model 4. The black curves are calculated with the exact reflection coefficient equation for VTI media, the green and red curves are respectively produced by Rüger equation and ASI Rüger equation. And the dot curves are obtained by the isotropic parts of the three equations mentioned above.

each subgraph of Figure 4, only one parameter is varied when the other seven are fixed. We can see that, for Rüger equation, there is strong relevance between vertical shear modulus, vertical P-wave velocity, and δ, specially, between vertical shear modulus and δ, and for ASI Rüger equation, there is strong relevance between vertical S-wave impedance and δ. The strong relevance will reduce the resolution between different parameters. But it does not mean that the parameters cannot be seprated absolutely. In orther to more quantitively investigate how strong the relevance is, in Figure 5, we display the coefficients of the parameters with strong relevance , which controls how the parameter variation impacts the PP-wave reflection coefficient. It shows that the vertical shear modulus and δ in Rüger equation are completely coupled, which means that they cannot be separated in the inverted results at all. However, there is still possible to separate the P-wave velocity from other parameters in Rüger equation, and to separate the P-wave impedance and δ in ASI Rüger equation. The similar discussion is also can be seen in (Plessix and Bork, 2000), however, in his equation, the S-wave impedance and δ are coupled, the density and ϵ are coupled.

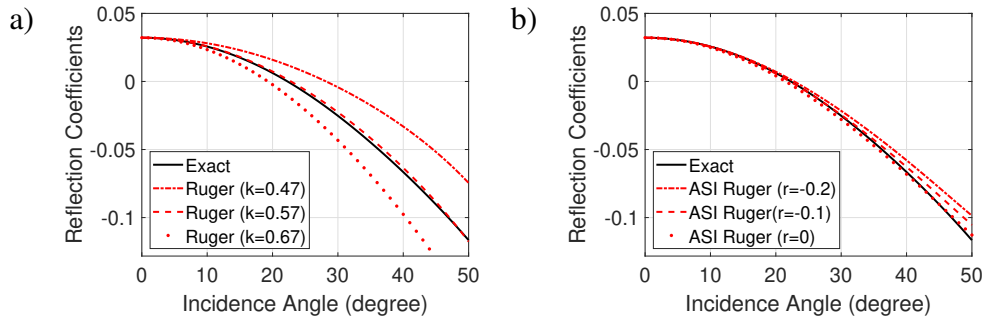

FIG. 2. Reflection coefficients of model 2, (a) calculated from Rüger equation using different k values, (b) calculated from ASI Rüger equation using different r values. The true k and r values for model 2 is 0.57 and -0.1, respectively.

Table 1. Models used to test the accuracy of ASI Rüger equation.

Model	Lithology	α(km/s)	β(km/s)	ρ(g/cm^3)	δ	ϵ
1	Shale	4.6	2.5	2.65	0.05	0.15
	Sand	5.5	3.5	2.7	0	0
2	Shale	4.6	2.5	2.65	0.05	0.15
	Sand	5.0	3.0	2.6	0	0
3	Shale	4.6	2.5	2.65	0.05	0.15
	Gas Shale	4.0	2.7	2.55	0	0
4		2.9	1.8	2.18	0	0
		3.1	1.85	2.2	0.2	0.1

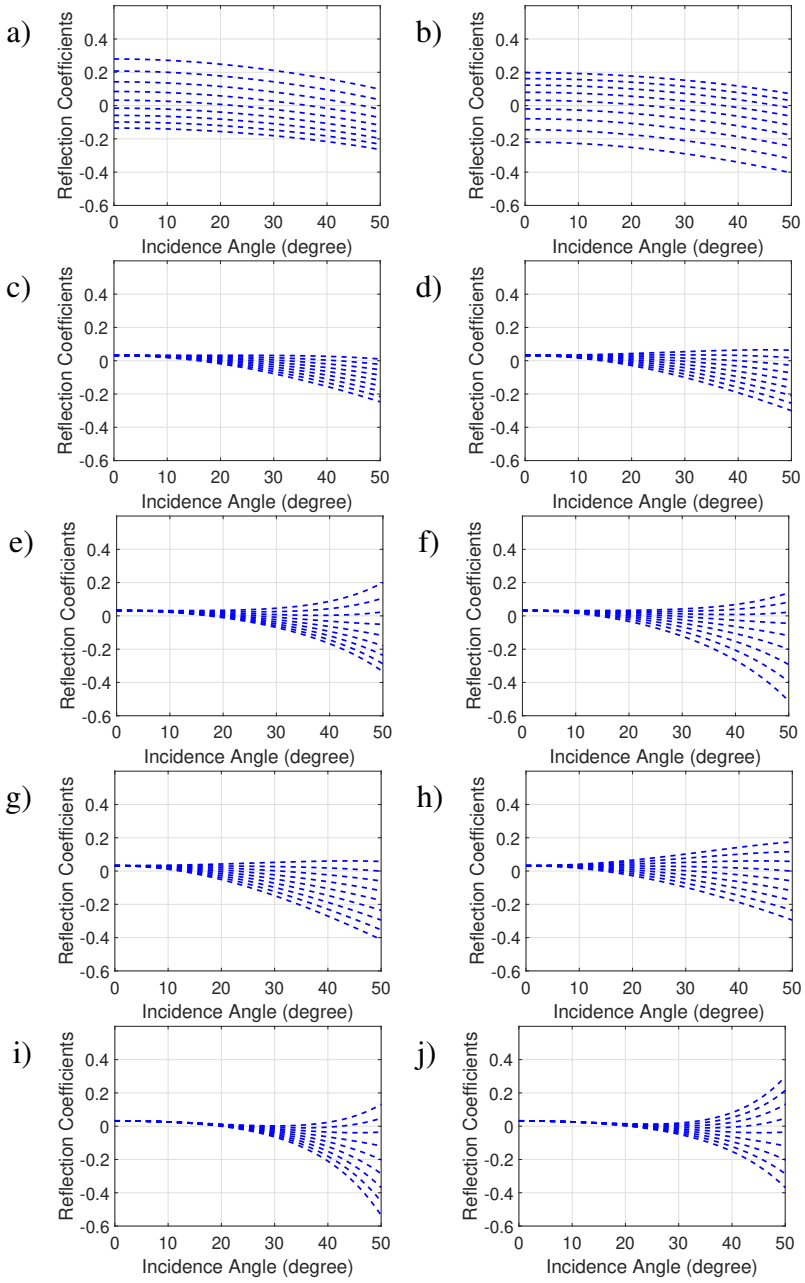

FIG. 3. The PP-wave reflection coefficients for model 2 in Table 1 using Rüger equation. The blue dash curves correspond differents parameters increased from -40 % to 40 % for nonanisotropic parameters (AI, μ, α), and from -0.8 to 0.8 for isotropic parameters (δ, ϵ). There are ten parameters totally, five for the upper layer and five for the below layer, and only one parameter is varied in each subgraph of Figure 3. (a), (b) Display the PP-wave reflection coefficients with varying vertical P-wave impedance of the upper layer and the below layer, respectively. (c), (d) Display the PP-wave reflection coefficients with varying vertical shear modulus of the upper layer and the below layer, respectively. (e), (f) Display the PP-wave reflection coefficients with varying vertical P-wave velocity of the upper layer and the below layer, respectively. (g), (h) Display the PP-wave reflection coefficients with varying δ of the upper layer and the below layer, respectively. (i), (j) Display the PP-wave reflection coefficients with varying ϵ of the upper layer and the below layer, respectively.

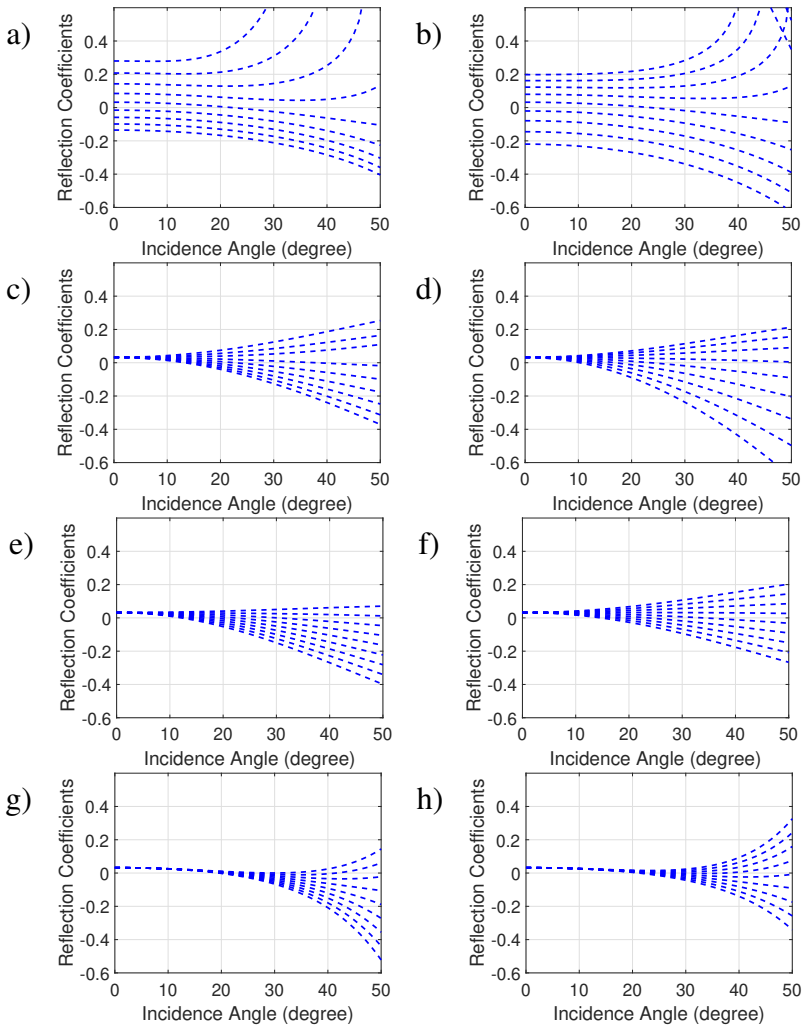

FIG. 4. The PP-wave reflection coefficients for model 2 in Table 1 using ASI Rüger equation. Figure 4 is similar with Figure 3, but using different parameters. (a), (b) Display the PP-wave reflection coefficients with varying vertical P-wave impedance of the upper layer and the below layer, respectively. (c), (d) Display the PP-wave reflection coefficients with varying vertical S-wave impedance of the upper layer and the below layer, respectively. (e), (f) Display the PP-wave reflection coefficients with varying δ of the upper layer and the below layer, respectively. (g), (h) Display the PP-wave reflection coefficients with varying ϵ of the upper layer and the below layer, respectively.

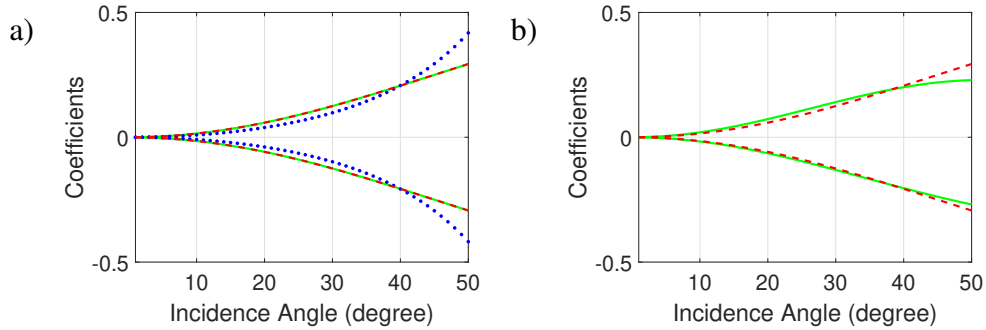

FIG. 5. Curves of the coefficients varies with incidence angle for the parameters with strong relevance. In Figure 5a or b, there are two curves for each color, one for the parameter of the upper layer in model 2 and one for the below layer in model 2. The coefficient curves for each layer are scaled to the same mean value. (a) Display the parameter coefficients in Rüger equation, the green curves are coefficients of the vertical shear modulus($\pm 2k^2 \sin^2\theta_i$), the blue dot curves are coefficients of the vertical P-wave velocity ($\mp\frac{1}{2}\tan^2\theta_i$), the red dash curves are coefficients of δ ($\mp\frac{1}{2}\sin^2\theta_i$). (b) Display the parameter coefficients in ASI Rüger equation, the green curves are coefficients of the vertical S-wave impedance (the partial derivative of ASI Rüger equation with respect to the vertical S-wave impedance, See appendix A), the red dash curves are coefficients of δ ($\mp\frac{1}{2}\sin^2\theta_i$).

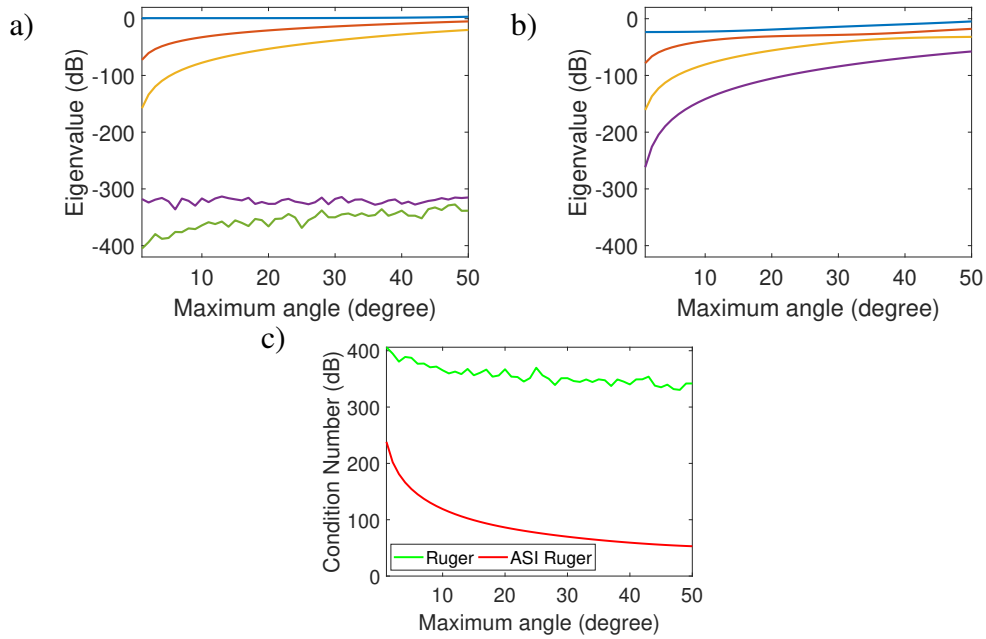

FIG. 6. (a) Eigenvalues of the Frechet matrix versus the maximum incidence angle for Rüger equation, from the top to bottom are the first to fifth eigenvalues. (b) Eigenvalues of the Frechet matrix versus the maximum incidence angle for ASI Rüger equation, from the top to bottom are the first to fourth eigenvalues. (c) The condition numbers versus the maximum incidence angle for Rüger equation (the green curve) and ASI Rüger equation (the red curve).

For a linear inversion problem of reflection amplitude data, which is expressed as:

$$\delta\mathbf{d} = \mathbf{F}\delta\mathbf{m}, \tag{20}$$

where $\delta\mathbf{d}$ represents data residue, $\mathbf{F}$ represents the sensitivity matrix of Fréchet derivatives of the model responses $\mathbf{d}(\mathbf{m})$ with respect to model parameters $\mathbf{m}$, and $\delta\mathbf{m}$ represents model perturbation. Here we only consider a single-interface model that is of two layers. For Rüger equation, the corresponding model parameters $\mathbf{m}$ of producing $\mathbf{F}$ is:

$$\mathbf{m} = [\frac{\Delta AI}{\overline{AI}}, \frac{\Delta\mu}{\overline{\mu}}, \frac{\Delta\alpha}{\overline{\alpha}}, \Delta\delta, \Delta\epsilon]. \tag{21}$$

For ASI Rüger equation, we assume the initial model:

$$\mathbf{m}_0 = [AI_1, SI_1, \delta_1, \epsilon_1], \tag{22}$$

then the corresponding model parameters $\mathbf{m}$ of producing $\mathbf{F}$ is:

$$\mathbf{m} = [AI_2, SI_2, \delta_2, \epsilon_2]. \tag{23}$$

The condition number of the sensitivity matrix (the ratio of the maximum eigenvalue to the minimum eigenvalue) is a measure of the ill-posedness of a inversion problem. And the ill-posedness of the problem increases with the increase of the condition number. Curves of the eigenvalues or condition numbers versus the maximum incidence angle for Rüger equation and ASI Rüger equation, respectively, are shown in Figure 6. In Figure 6a, the fourth and fifth eigenvalues corresponding the anisotropic parameters are on a fairly low level compared with that corresponding the other parameters, which causes that the anisotropic parameters become too difficult to inverse. Differently, in figure 6b, all the eigenvalues for ASI Rüger equation are on close levels, it means that the difficulties for inversing different parameters are not so different. Figure 6c illustrates that the inversion based on ASI Rüger equation can reduce the ill-posedness, because of the significant decrease of the condition number.

SYNTHETIC DATA EXAMPLE

In order to verify the stability and reliability of the method, a real log data is used as a true model displayed in Figure 7a, and the convolution method and exact reflection coefficient equation are employed to generate the synthetic data displayed in Figure 7b. The maximum incidence angle is 40 degrees. In Figure 8a-c, we show the results of simultaneous inversion using synthetic data with different levels of Gauss noise. Figure 8a displays the inverted results using free noise synthetic data, Figure 2b, 2c are the inverted results using synthetic data with the signal to noise ratio(SNR) of 4:1, and 1:1, respectively. The inversion results show that, even under the condition of high noise, the proposed method can stably and reliably invert the vertical P-wave impedance, the vertical S-wave impedance, and the anisotropic parameters δ, ϵ. To investigate how the constant assumption impacts the inverted results, in Figure 9, we display the inverted results with different r values (-0.3, -0.17, and 0), and the mean value for the true model is -0.17. It shows that a reasonable error on the constant has little effect on the results.

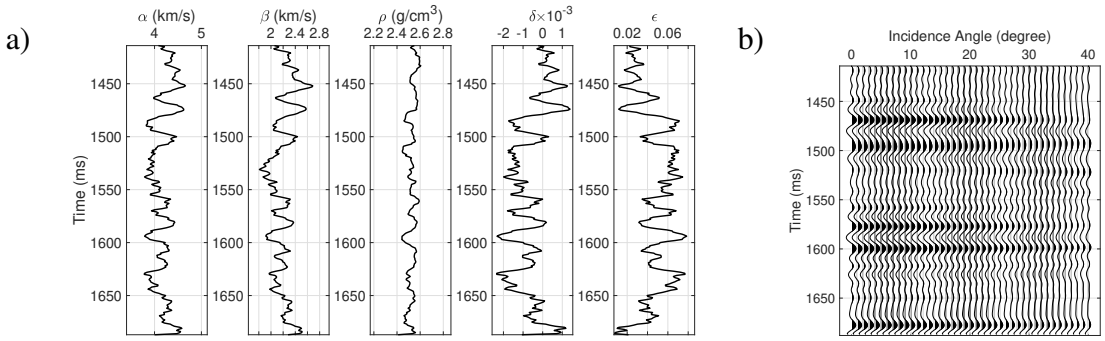

FIG. 7. (a) The true models from well logs. (b) Noise free synthetic data.

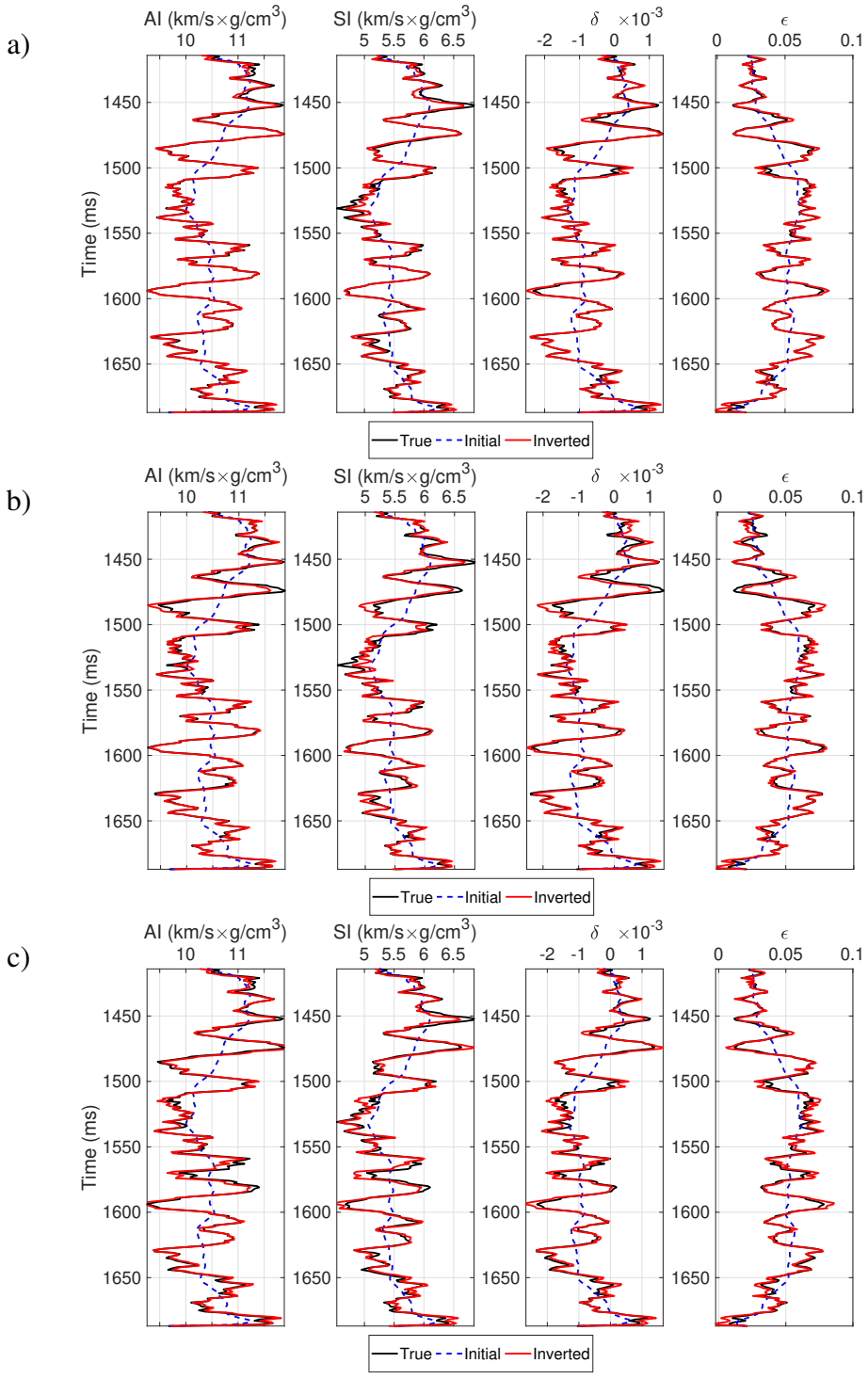

FIG. 8. The black solid curves are true models from well logs, The blue dash curves are initial models, the red solid curves are inverted results. (a) The inverted results using noise free synthetic data. (b) The inverted results using synthetic data with the the signal to noise ration (SNR) 4:1. (c) The inverted results using synthetic data with the signal to noise ration (SNR) 1:1.

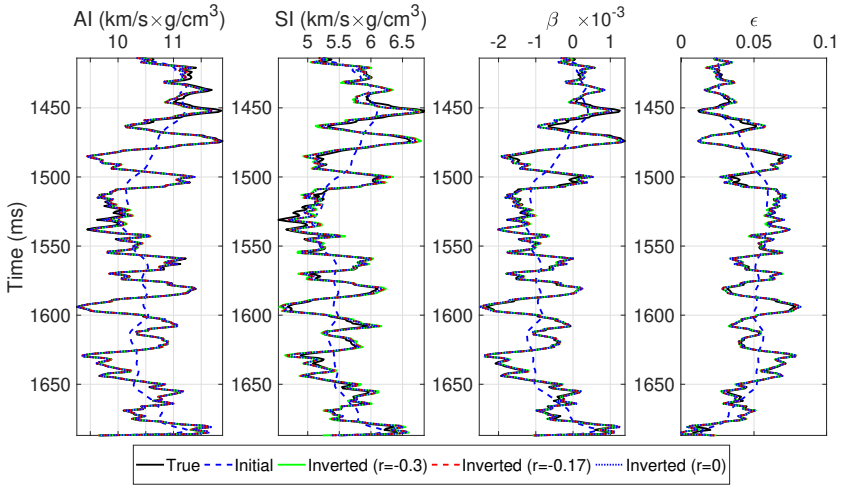

FIG. 9. Inverted results using free noise data with different r values. The black solid curves are true models, the blue dash curves are initial models, the green solid curves are inverted results with r value of -0.3, the red dash curves are inverted results with r value of -0.17, the blue dot curves are inverted results with r value of 0.

CONCLUSION

In this paper we realized the simultaneous AVO inversion of anisotropic parameters for the transversely isotropic media with vertical axis of symmetry (VTI media). First we introduce a nonlinear PP-wave reflection coefficient approximation equation (ASI equation) for isotropic elastic media, then by replacing the isotropic part of Rüger equation with this equation, we obtain a new reflection coefficient approximation equation (ASI Rüger equation) for VTI media. In order to invert the VTI parameters based on ASI Rüger equation, we develop the Bayesian generalized linear inversion (BGLI), in which the noise and model perturbation are assumed to conform to the zero mean Gaussian distribution.

ASI Rüger equation can express the PP-wave reflection coefficient in VTI media well. Compared with Rüger equation, ASI Rüger equation is less sensitivity to the bias in the intrinsic constant, lowers the relevance between the parameters, reduces the ill-posedness of inversion problem. The synthetic data test shows that the proposed mothed can stably and reliably invert VTI parameters (the vertical P-wave impedance, the vertical S-wave impedance, δ, and ϵ) , and the inverted results are almost unaffected by the errors on the intrinsic constant. But there is still a strong relevance between the vertical S-wave impedance and δ, it could be a potential risk on the results. In addition, based on our experience, if we utilize the P-wave incidence angle instead of the transmission angle in anisotropic background medium calculated by equation 19 , the effect of the results are very small in the case of weak impedance contrast, the calculation of the transmission angle can be avoided.

ACKNOWLEDGEMENTS

We thank the sponsors of CREWES for continued support. This work was funded by CREWES industrial sponsors, and NSERC (Natural Science and Engineering Research Council of Canada) through the grant CRDPJ 461179-13.

REFERENCES

Aki, K., and Richards, P. G., 2002, Quantitative seismology:

Banik, N., 1987, An effective anisotropy parameter in transversely isotropic media: Geophysics, **52**, No. 12, 1654–1664.

Bortfeld, R., 1961, Approximations to the reflection and transmission coefficients of plane longitudinal and transverse waves: Geophysical Prospecting, **9**, No. 4, 485–502.

Carcione, J. M., Helle, H. B., and Zhao, T., 1998, Effects of attenuation and anisotropy on reflection amplitude versus offset: Geophysics, **63**, No. 5, 1652–1658.

Castagna, J. P., and Backus, M. M., 1993, Offset-dependent reflectivity—Theory and practice of AVO analysis: Society of Exploration Geophysicists.

Cooke, D. A., and Schneider, W. A., 1983, Generalized linear inversion of reflection seismic data: Geophysics, **48**, No. 6, 665–676.

Daley, P. F., and Hron, F., 1977, Reflection and transmission coefficients for transversely isotropic media: Bulletin of the seismological society of America, **67**, No. 3, 661–675.

Fatti, J. L., Smith, G. C., Vail, P. J., Strauss, P. J., and Levitt, P. R., 1994, Detection of gas in sandstone reservoirs using avo analysis: A 3-d seismic case history using the geostack technique: Geophysics, **59**, No. 9, 1362–1376.

Fryer, G. J., and Frazer, L. N., 1984, Seismic waves in stratified anisotropic media: Geophysical Journal International, **78**, No. 3, 691–710.

Fu, X., Zhang, F., and Li, X.-Y., 2017, Simultaneous inversion of p-and s-wave impedance based on an improved avo equation, *in* SEG Technical Program Expanded Abstracts 2017, Society of Exploration Geophysicists, 828–833.

Fu, X., Zhang, F., Li, X.-Y., Qian, Z., Chen, H., and Mei, L., 2019, Simultaneous inversion of p- and s-wave impedances based on an improved approximation equation of reflection coefficient: Chinese Journal of Geophysics (in Chinese), **62**, No. 1, 276–288.

Fu, X., Zhang, F., Li, X.-Y., Yang, S., and Ma, G.-R., 2018, Simultaneous inversion of p-wave impedance and the ratio of s-to p-wave velocity, *in* International Geophysical Conference, Beijing, China, 24-27 April 2018, Society of Exploration Geophysicists and Chinese Petroleum Society, 1193–1196.

Gholami, A., Aghamiry, H. S., and Abbasi, M., 2018, Constrained nonlinear amplitude variation with offset inversion using zoeppritz equations: Geophysics, **83**, No. 3, R245–R255.

Gidlow, P., Smith, G., and Vail, P., 1992, Hydrocarbon detection using fluid factor traces: A case history: Presented at the joint society of exploration geophysicists, *in* EAGE Summer Research Workshop on "How useful is amplitude-versus-offset (AVO) analysis, 78–89.

Goodway, B., Chen, T., and Downton, J., 1997, Improved avo fluid detection and lithology discrimination using lamé petrophysical parameters;"$\lambda\rho$","$\mu\rho$", & "λ/μ fluid stack", from p and s inversions, *in* SEG Technical Program Expanded Abstracts 1997, Society of Exploration Geophysicists, 183–186.

Graebner, M., 1992, Plane-wave reflection and transmission coefficients for a transversely isotropic solid: Geophysics, **57**, No. 11, 1512–1519.

Gray, D., Goodway, B., and Chen, T., 1999, Bridging the gap: Using avo to detect changes in fundamental elastic constants, *in* SEG Technical Program Expanded Abstracts 1999, Society of Exploration Geophysicists, 852–855.

Hilterman, F. J., 2001, Seismic Amplitude Interpretation: 2001 Distinguished Instructor Short Course, 4: SEG Books.

Innanen, K. A., 2011, Inversion of the seismic avf/ava signatures of highly attenuative targets: Geophysics, **76**, No. 1, R1–R14.

Innanen, K. A., 2013, Coupling in amplitude variation with offset and the wiggins approximation: Geophysics, **78**, No. 4, N21–N33.

Innanen, K. A., and Mahmoudian, F., 2015, Characterizing the degree of amplitude-variation-with-offset nonlinearity in seismic physical modelling reflection data: Geophysical Prospecting, **63**, No. 1, 133–140.

Jin, S., and Stovas, A., 2019, Reflection and transmission responses for layered transversely isotropic media with vertical and horizontal symmetry axes: Geophysics, **84**, No. 4, C181–C203.

Keith, C. M., and Crampin, S., 1977, Seismic body waves in anisotropic media: reflection and refraction at a plane interface: Geophysical Journal International, **49**, No. 1, 181–208.

Kim, K. Y., Wrolstad, K. H., and Aminzadeh, F., 1993, Effects of transverse isotropy on p-wave avo for gas sands: Geophysics, **58**, No. 6, 883–888.

Lin, R., and Thomsen, L., 2013, Extracting polar anisotropy parameters from seismic data and well logs, *in* SEG Technical Program Expanded Abstracts 2013, Society of Exploration Geophysicists, 310–314.

Liu, F., Meng, X., Wang, Y., Shen, G., and Yang, C., 2011, Jacobian matrix for the inversion of p-and s-wave velocities and its accurate computation method: Science China Earth Sciences, **54**, No. 5, 647–654.

Ma, J., 2003, Forward modeling and inversion methods based on generalized elastic impedance in seismic exploration: Chinese Journal of Geophysics, **46**, No. 1, 159–168.

Ma, J., Fu, G., Geng, J., and Guo, T., 2013, Full zoeppritz equation-based elastic parameters bayesian generalized linear inversion, *in* 75th EAGE Conference & Exhibition incorporating SPE EUROPEC 2013.

Mallick, S., 1993, A simple approximation to the p-wave reflection coefficient and its implication in the inversion of amplitude variation with offset data: Geophysics, **58**, No. 4, 544–552.

Pan, X.-P., Zhang, G.-Z., Zhang, J.-J., and Yin, X.-Y., 2017, Zoeppritz-based avo inversion using an improved markov chain monte carlo method: Petroleum science, **14**, No. 1, 75–83.

Plessix, R.-E., and Bork, J., 2000, Quantitative estimate of vti parameters from ava responses: Geophysical Prospecting, **48**, No. 1, 87–108.

Potter, C., and Stewart, R., 1998, Density predictions using vp and vs sonic logs: CREWES Res. Rep, **10**, 1–10.

Richards, P. G., and Frasier, C. W., 1976, Scattering of elastic waves from depth-dependent inhomogeneities: Geophysics, **41**, No. 3, 441–458.

Rüger, A., 1997, P-wave reflection coefficients for transversely isotropic models with vertical and horizontal axis of symmetry: Geophysics, **62**, No. 3, 713–722.

Rüger, A., 1998, Variation of p-wave reflectivity with offset and azimuth in anisotropic media: Geophysics, **63**, No. 3, 935–947.

Russell, B. H., Gray, D., and Hampson, D. P., 2011, Linearized avo and poroelasticity: Geophysics, **76**, No. 3, C19–C29.

Rutherford, S. R., and Williams, R. H., 1989, Amplitude-versus-offset variations in gas sands: Geophysics, **54**, No. 6, 680–688.

Schoenberg, M., and Protazio, J., 1992, 'zoeppritz' rationalized, and generalized to anisotropic: Journal of Seismic Exploration, **1**, No. 2, 125–144.

Shuey, R., 1985, A simplification of the zoeppritz equations: Geophysics, **50**, No. 4, 609–614.

Smith, G., and Gidlow, P., 1987, Weighted stacking for rock property estimation and detection of gas: Geophysical Prospecting, **35**, No. 9, 993–1014.

Stovas, A., Landrø, M., and Avseth, P., 2006, Avo attribute inversion for finely layered reservoirs: Geophysics, **71**, No. 3, C25–C36.

Stovas, A., and Ursin, B., 2001, Second-order approximations of the reflection and transmission coefficients between two visco-elastic isotropic media: Journal of Seismic Exploration, **9**, No. 3, 223–233.

Stovas, A., and Ursin, B., 2003, Reflection and transmission responses of layered transversely isotropic viscoelastic media: Geophysical Prospecting, **51**, No. 5, 447–477.

Thomsen, L., 1986, Weak elastic anisotropy: Geophysics, **51**, No. 10, 1954–1966.

Ursenbach, C. P., 2002, Optimal zoeppritz approximations, *in* SEG Technical Program Expanded Abstracts 2002, Society of Exploration Geophysicists, 1897–1900.

Vavrycuk, V., and Psencik, I., 1998, Pp-wave reflection coefficients in weakly anisotropic elastic media: Geophysics, **63**, No. 6, 2129–2141.

Wang, Y., 1999, Approximations to the zoeppritz equations and their use in avo analysis: Geophysics, **64**, No. 6, 1920–1927.

Wang, Y., 2003, Seismic amplitude inversion in reflection tomography, vol. 33: Elsevier.

Wei, X., and Chen, T., 2011, Joint pp and ps avo inversion based on zoeppritz equations: Earthquake Science, **24**, No. 4, 329–334.

Wiggins, R., Kenny, G. S., and McClure, C. D., 1983, A method for determining and displaying the shear-velocity reflectivities of a geologic formation: European patent application, **113944**.

Wright, J., 1987, The effects of transverse isotropy on reflection amplitude versus offset: Geophysics, **52**, No. 4, 564–567.

Zhang, F., and Li, X., 2013, Generalized approximations of reflection coefficients in orthorhombic media: Journal of Geophysics and Engineering, **10**, No. 5, 054,004.

Zhang, F., Zhang, T., and Li, X.-Y., 2019, Seismic amplitude inversion for the transversely isotropic media with vertical axis of symmetry: Geophysical Prospecting.

Zhi, L., Chen, S., and Li, X.-y., 2016, Amplitude variation with angle inversion using the exact zoeppritz equations—theory and methodology: Geophysics, **81**, No. 2, N1–N15.

Zhou, L., Li, J., Chen, X., Liu, X., and Chen, L., 2017, Prestack amplitude versus angle inversion for young's modulus and poisson's ratio based on the exact zoeppritz equations: Geophysical Prospecting, **65**, No. 6, 1462–1476.

Zhu, X., and McMechan, G., 2012, Avo inversion using the zoeppritz equation for pp reflections, *in* SEG Technical Program Expanded Abstracts 2012, Society of Exploration Geophysicists, 1–5.

Zillmer, M., Gajewski, D., and Kashtan, B. M., 1998, Anisotropic reflection coefficients for a weak-contrast interface: Geophysical Journal International, **132**, No. 1, 159–166.

Zoeppritz, K., 1919, Erdbebenwellen viii b: On the reflection and penetration of seismic waves through unstable layers: Goettinger nachrichten.

Zong, Z., Yin, X., and Wu, G., 2013, Elastic impedance parameterization and inversion with young's modulus and poisson's ratio: Geophysics, **78**, No. 6, N35–N42.

Zong, Z., Yin, X., and Wu, G., 2015, Geofluid discrimination incorporating poroelasticity and seismic reflection inversion: Surveys in Geophysics, **36**, No. 5, 659–681.

APPENDIX A. EXPRESSIONS OF SYMBLES IN EQUATION 12

The observed data:

$$\mathbf{d}(\mathbf{m}) = [\mathbf{S}(\theta_1), \mathbf{S}(\theta_2), \cdots, \mathbf{S}(\theta_n)]^T, \tag{A.1}$$

where

$$\mathbf{S}(\theta_n) = [S_1(\theta_n), S_2(\theta_n), \cdots, S_l(\theta_n)], \tag{A.2}$$

where $\mathbf{S}(\theta_i)$ is a single trace of the angle gather profile with the incident angle θ_i, $S_j(\theta_i)$ is the j^{th} seismic sample in the trace, n is the number of angles and l is the sampling number of the trace. The model to be solved and the initial model:

$$\mathbf{m} = [\mathbf{AI}, \mathbf{SI}, \boldsymbol{\delta}, \boldsymbol{\epsilon}]^T, \tag{A.3}$$

$$\mathbf{m}_0 = [\mathbf{AI}_0, \mathbf{SI}_0, \boldsymbol{\delta}_0, \boldsymbol{\epsilon}_0]^T \tag{A.4}$$

where

$$\mathbf{AI} = [AI_1, AI_2, \cdots, AI_l, AI_{l+1}], \tag{A.5}$$

$$\mathbf{SI} = [SI_1, SI_2, \cdots, SI_l, SI_{l+1}], \tag{A.6}$$

$$\boldsymbol{\delta} = [\delta_1, \delta_2, \cdots, \delta_l, \delta_{l+1}], \tag{A.7}$$

$$\boldsymbol{\epsilon} = [\epsilon_1, \epsilon_2, \cdots, \epsilon_l, \epsilon_{l+1}], \tag{A.8}$$

$$\mathbf{AI}_0 = [AI_{01}, AI_{02}, \cdots, AI_{0l}, AI_{0l+1}], \tag{A.9}$$

$$\mathbf{SI}_0 = [SI_{01}, SI_{02}, \cdots, SI_{0l}, SI_{0l+1}], \tag{A.10}$$

$$\boldsymbol{\delta}_0 = [\delta_{01}, \delta_{02}, \cdots, \delta_{0l}, \delta_{0l+1}], \tag{A.11}$$

$$\boldsymbol{\epsilon}_0 = [\epsilon_{01}, \epsilon_{02}, \cdots, \epsilon_{0l}, \epsilon_{0l+1}], \tag{A.12}$$

where m_i and m_{0i} ($m = AI, SI, \delta, or\ \epsilon$) is the model parameter to solve and the initial model parameter, respectively, of the i^{th} layer. The model perturbation:

$$\Delta\mathbf{m} = \mathbf{m} - \mathbf{m}_0 = [\Delta\mathbf{AI}, \Delta\mathbf{SI}, \Delta\boldsymbol{\delta}, \Delta\boldsymbol{\epsilon}]^T \tag{A.13}$$

where

$$\Delta\mathbf{AI} = \mathbf{AI} - \mathbf{AI}_0, \Delta\mathbf{SI} = \mathbf{SI} - \mathbf{SI}_0, \Delta\boldsymbol{\delta} = \boldsymbol{\delta} - \boldsymbol{\delta}_0, \Delta\boldsymbol{\epsilon} = \boldsymbol{\epsilon} - \boldsymbol{\epsilon}_0. \tag{A.14}$$

The Jacobian matrix:

$$\frac{\partial \mathbf{d}(\mathbf{m}_0)}{\partial \mathbf{m}_0} = \begin{bmatrix} \mathbf{W}_1\mathbf{B}_1 & \mathbf{W}_1\mathbf{B}_1 & \mathbf{W}_1\mathbf{C}_1 & \mathbf{W}_1\mathbf{D}_1 \\ \mathbf{W}_2\mathbf{B}_2 & \mathbf{W}_2\mathbf{B}_2 & \mathbf{W}_2\mathbf{C}_2 & \mathbf{W}_2\mathbf{D}_2 \\ \vdots & \vdots & \vdots & \vdots \\ \mathbf{W}_n\mathbf{B}_n & \mathbf{W}_n\mathbf{B}_n & \mathbf{W}_n\mathbf{C}_n & \mathbf{W}_n\mathbf{D}_n \end{bmatrix}, \tag{A.15}$$

where

$$\mathbf{W}_i = \begin{bmatrix} w_{\theta_i}(1*\Delta t) & 0 & \cdots & 0 \\ w_{\theta_i}(2*\Delta t) & w_{\theta_i}(1*\Delta t) & \cdots & 0 \\ \vdots & w_{\theta_i}(2*\Delta t) & \ddots & 0 \\ w_{\theta_i}(l*\Delta t) & \vdots & \ddots & w_{\theta_i}(1*\Delta t) \\ 0 & w_{\theta_i}(l*\Delta t) & \ddots & w_{\theta_i}(2*\Delta t) \\ 0 & 0 & \ddots & \vdots \\ 0 & 0 & 0 & w_{\theta_i}(l*\Delta t) \end{bmatrix}_{l\times l}, \tag{A.16}$$

where w_{θ_i} is the source wavelet function corresponding to the angle gather with P-wave incidence angle θ_i, and Δt is the sampling interval. In formula A.15, $\mathbf{A}_i$, $\mathbf{B}_i$, $\mathbf{C}_i$, and $\mathbf{D}_i$ are $l \times (l+1)$ matrices, the elements in them are, respectively:

$$\begin{aligned} \mathbf{A}_i(j,k) = &\frac{\partial R_{ASI}^{VTI}(\theta_i, \mathbf{m}')}{\partial AI_1}|_{\mathbf{m}'=\mathbf{m}_0'} \times \delta\{j-k\} \\ &+ \frac{\partial R_{ASI}^{VTI}(\theta_i, \mathbf{m}')}{\partial AI_2}|_{\mathbf{m}'=\mathbf{m}_0'} \times \delta\{j-(k-1)\}, \end{aligned} \tag{A.17}$$

$$\begin{aligned}\mathbf{B}_i(j,k) = &\frac{\partial R_{ASI}^{VTI}(\theta_i,\mathbf{m}')}{\partial SI_1}|_{\mathbf{m}'=\mathbf{m}_0'} \times \delta\{j-k\} \\ &+ \frac{\partial R_{ASI}^{VTI}(\theta_i,\mathbf{m}')}{\partial SI_2}|_{\mathbf{m}'=\mathbf{m}_0'} \times \delta\{j-(k-1)\},\end{aligned} \tag{A.18}$$

$$\begin{aligned}\mathbf{C}_i(j,k) = &\frac{\partial R_{ASI}^{VTI}(\theta_i,\mathbf{m}')}{\partial \delta_1}|_{\mathbf{m}'=\mathbf{m}_0'} \times \delta\{j-k\} \\ &+ \frac{\partial R_{ASI}^{VTI}(\theta_i,\mathbf{m}')}{\partial \delta_2}|_{\mathbf{m}'=\mathbf{m}_0'} \times \delta\{j-(k-1)\},\end{aligned} \tag{A.19}$$

$$\begin{aligned}\mathbf{D}_i(j,k) = &\frac{\partial R_{ASI}^{VTI}(\theta_i,\mathbf{m}')}{\partial \epsilon_1}|_{\mathbf{m}'=\mathbf{m}_0'} \times \delta\{j-k\} \\ &+ \frac{\partial R_{ASI}^{VTI}(\theta_i,\mathbf{m}')}{\partial \epsilon_2}|_{\mathbf{m}'=\mathbf{m}_0'} \times \delta\{j-(k-1)\},\end{aligned} \tag{A.20}$$

where $\mathbf{m}' = [AI_1, SI_1, \delta_1, \epsilon_1, AI_2, SI_2, \delta_2, \epsilon_2]$, $\mathbf{m}_0' = [AI_j, SI_j, \delta_j, \epsilon_j, AI_k, SI_k, \delta_k, \epsilon_k]$, $R_{ASI}^{VTI}(\theta_i)$ is ASI Rüger equation, $\delta\{\cdot\}$ is Dirac delta function, $j = 1, 2, \cdots, l$ and $k = 1, 2, \cdots, l, l+1$.